AN ABSTRACT OF THE THESIS OF

Victor Brequigny for the degree of Bahcelor of Science in Physics presented on May 18, 2019.

Title: Terahertz field enhancement in nanoantennas on gallium arsenide.

Abstract approved: _____

Yun-Shik Lee

Terahertz (THz) spectroscopy is a great tool not only to study fundamental physical processes such as many-body Coulomb interaction but also to develop ultrafast electronic devices. More specifically, intense THz fields interacting with semiconductors have exhibited strong nonlinear effect involving extreme carrier dynamics. In this experiment, intense THz radiation was applied to nanoantennas on a gallium arsenide wafer. The nanoantenna structure causes the incident THz field to be tremendously enhanced (field enhancement factor, $\alpha \cong 50$). This huge field enhancement allows the THz fields to generate charge carriers of high density ($Ne > 10^{20}$) via interbrand excitation associated with Zener tunneling and impact ionization. The high-density free electrons induce strong THz absorption, up to 35%. This shows the potential application of metal-semiconductor hybrid nanostructure in the development of optical modulators and active switching devices.

Terahertz field enhancement in nanoantennas on gallium arsenide.

by

Victor Brequigny

A THESIS

submitted to

Oregon State University

in partial fulfillment of
the requirements for the
degree of

Bachelor of Science

Presented May 18, 2019
Commencement June 2019

Bachelor of Science thesis of Victor Brequigny presented on May 18, 2019.

APPROVED:

Major Professor, representing Physics

Director of the School of Physics

I understand that my thesis will become part of the permanent collection of Oregon State University libraries. My signature below authorizes release of my thesis to any reader upon request.

Victor Brequigny, Author

Contents

List of Figures

Chapter 1

Introduction

Terahertz (THz) spectroscopy is a new emerging field that has a promising future. Photons of THz electromagnetic (EM) waves have an energy that matches the energy difference between states in condensed matter. This property makes THz spectroscopy extremely useful in the study of the quantum properties of many-body systems. Gaining this kind of information of the electronic dynamics in semiconductors can be used to design new technologies that can be controlled up to the quantum levels. Consequently THz spectroscopy has great possible application for the development of ultrafast optoelectronics devices. In the quest of designing the transducers of tomorrow, components properties must be explored in extreme cases. In addition, nano devices will have internal electric field that can exceed MV/cm, therefore it is crucial that researchers recreate such intense fields when studying the properties of semiconductors. Recently some researchers have used small rectangular holes to greatly enhance the near electric field. [1, 2] Combined with THz spectroscopy this offers new way to investigate the carrier dynamics of semiconductors used in current devices.

There are now multiple ways to generate high power terahertz (THz) radiation. The technique we favored uses high intensity femtoseconds laser pulses inside a nonlinear crystal (lithium niobate) to generate THz pulses. Lithium niobate lacks inversion symmetry, therefore the electrons from the incident optical pulse experience a noncentrosymmetric potential. Their oscillation then become more complex and they exhibit nonlinear features. Their equation of motion is well modeled by an anharmonic oscillator. That equation is solved using

perturbation theory. One of the second order response obtained by the perturbation theory is called optical rectification. This nonlinear optical effect induces a bulk polarization that varies through time which generates electromagnetic radiation. The spectral bandwidth of such radiation is approximately the inverse of the optical pulse duration. Consequently, high power femtosecond pulses can generate THz pulses inside a noncentrosymetric medium such lithium niobate [3].

The THz and the optical pulses inside the crystal have different refractive indices. The index of refraction of the Thz pulse being greater than the one for the optical pulses the phase velocity of the THz will then travel slower than the group velocity of the optical pulse. Because of this difference of velocity the THz pulses generated by the optical pulse inside the crystal will destructively interfere with its predecessor causing the THz radiation to vanish. One popular solution to this problem is to tilt the optical pulse front prior to entering lithium niobate using a diffraction grating. The optical pulse is tilted to be perpendicular to the propagation direction of the THz pulse by establishing the velocity matching condition between the two pulses [4].

Chapter 2

Terahertz Nanoantennas

2.1 Nanoantenna Array

We employed nanoslot antennas to acheive extremely high THz fields in semiconductors. As Figure 2.1 represent the nanoantenna array was etched out from a 100 nm thick gold / 3 nm thick Ti adhesion layer that was placed on top of a 0.5 mm thick single crystal intrinsic GaAs.

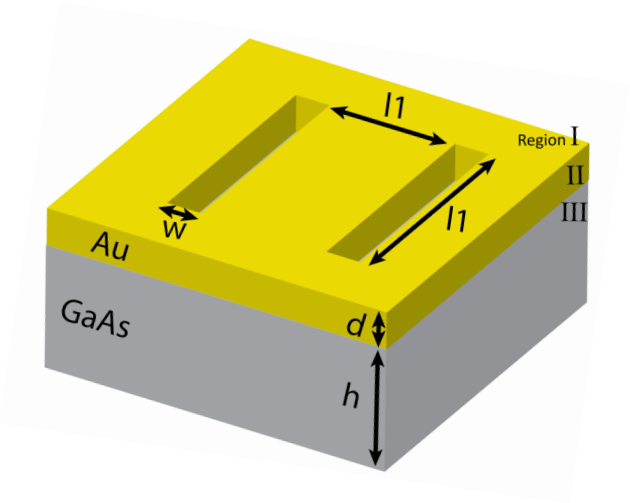

Figure 2.1: **Nano-slot-antenna-array-patterned GaAs sample**: the dimensions are $l_1 = 60\mu$m, and $w = 200$nm. The thickness of the gold layer is $d = 100$nm and the thickness of the gallium arsenide is 0.5 mm. This representation is not to scale, only a couple of nanoantennas were represented for clarity.

Each nanoantenna is a rectangular hole with a width w of 200 nm and a length l_1 of 60 μm placed at the center of a 60 $\times$ 70 μm^2 unit cell. All antennas are contained in an array of 5 mm by 5 mm. This ensures that the array is larger than the incident THz beam diameter.

2.2 Shape Resonance

2.2.1 Rayleigh wave expansion

Our goal is to find expressions for the electric field in all regions (labeled in Figure 2.1) and to observe any exhibition of field enhancement. There are different ways to go about this. Here we favored using the Rayleigh wave expansion and waveguide mode expansion derived by Park *et al.* [1]. The geometry of the antennas is very important in order to obtain the EM fields. The rectangular holes are aligned so that the reciprocal vectors are given by $\alpha_x = \frac{2\pi}{dx}$ and $\beta_y = \frac{2\pi}{dy}$. Those vectors are components of the EM wavevectors and are the base vectors of the Fourier component of the EM waves. Then using the Rayleigh wave expansion the magnetic field in Region I and III is expressed by

$$\left(H_x^I, H_y^I, H_z^I\right) = \sqrt{\frac{\epsilon_0}{\mu_0}} \sum_{mn} \left(G_{mm}^x, G_{mm}^y, G_{mm}^z\right) \times e^{i\chi_{mn}\left(z-\frac{h}{2}\right)} \times e^{i(\phi_{mn}-\omega t)} + e^{ik\left(z-\frac{h}{2}\right)}. \quad (2.1)$$

$$\left(H_x^{III}, H_y^{III}, H_z^{III}\right) = \sqrt{\frac{\epsilon_0}{\mu_0}} \sum_{mn} \left(F_{mm}^x, F_{mm}^y, F_{mm}^z\right) \times e^{-i\chi_{mn}\left(z-\frac{h}{2}\right)} \times e^{i(\phi_{mn}-\omega t)}. \quad (2.2)$$

where G and F are the Fourier amplitudes for the reflected and transmitted region, respectively. ϕ_{mn} is a spatial phase components on the xy-plane and is expressed by $\phi_{mn} = \alpha_m x + \beta_n y$. χ_{mn} is a wavevector along the z-direction and is given by $\chi_{mn}^2 = k^2 - \alpha_m^2 + \beta_n^2$. ϵ_0 is the vacuum permeability and μ_0 the permittivity. Here the magnetic field is used rather than the electric field as it simplifies the boundary condition calculation. Now that we have an expression for the transverse magnetic (TM) EM wave in both the reflected and transmitted region the next step is to find an expression for it inside the second region.

2.2.2 Waveguide mode expansion

While equation 2.1 and 2.2 were found using the Rayleigh wave expansion the magnetic field in region II can be found using the waveguide mode expansion. Hence the general expression for H inside the antenna:

$$\vec{H} = (H_x, H_y, H_z) = \sum_{ij} \left(H_{ij}^{ox}, H_{ij}^{oy}, H_{ij}^{oz}\right) \times e^{i(\mu_{ij} z - \omega t)}. \tag{2.3}$$

This expression is general and can be simplified using the properties of the antennas. μ_{ij} is a wavevector along z and is given by $\mu_{ij} = \sqrt{k^2 - (k_x^i)^2 - (k_x^j)^2}$ with the following reciprocal vectors: $k_x^i = \pi i/w$ and $k_x^j = \pi j/l$. The incident wavelength is larger than l, and especially w. This causes k_x^i and k_x^j to be greater than $\mathbf{k}$, therefore making μ_{ij} imaginary. Since k_x^i is significantly larger than $\mathbf{k}$, the contribution from the terms $i > 0$ are negligible since $e^{-|\mu_{ij}|z}$ decays fast. Similarly, the $j > 1$ terms can also be neglected. Therefore μ_{01} becomes $\mu_{01} = \sqrt{k^2 - (\pi/l)^2}$ In the end only the TM_{01} mode will appear. This approximation yields the following expression for the magnetic field in region II

$$H_x^{II} = 0. \tag{2.4}$$

$$H_y^{II} = -\frac{i\mu}{k}\sqrt{\frac{\epsilon_0}{\mu_0}} \sin\left(\frac{\pi y}{l}\right) \times \left(A\frac{\sin \mu z}{\sin\left(\frac{\mu h}{2}\right)} + B\frac{\cos \mu z}{\cos\left(\frac{\mu h}{2}\right)}\right). \tag{2.5}$$

$$H_z^{II} = \frac{i}{k}\frac{\pi}{b}\sqrt{\frac{\epsilon_0}{\mu_0}} \cos\left(\frac{\pi y}{l}\right) \times \left(-A\frac{\cos \mu z}{\sin\left(\frac{\mu h}{2}\right)} + B\frac{\sin \mu z}{\cos\left(\frac{\mu h}{2}\right)}\right). \tag{2.6}$$

where $\mu = \mu_{01}$ for clairity. Also, A and B denote the waveguide mode amplitudes.

2.2.3 Boundary conditions

Equation 2.1, 2.2, 2.5, and 2.6 gave us four unknown Fourier amplitude G, F, A, and B. The following boundary conditions are applied in order to solve for the amplitudes

$$\begin{cases} \dfrac{\partial H_z}{\partial y} - \dfrac{\partial H_y}{\partial z}\Big|_{III} = \dfrac{\partial H_z}{\partial y} - \dfrac{\partial H_y}{\partial z}\Big|_{II} \\ -\dfrac{\partial H_z}{\partial x} - \dfrac{\partial H_x}{\partial z}\Big|_{III} = \dfrac{\partial H_z}{\partial x} - \dfrac{\partial H_x}{\partial z}\Big|_{II} \end{cases} \text{ at } z = -h/2, \tag{2.7}$$

$$H_y^{III} = H_y^{II} \text{ at } 0 \le x \le w,\ 0 \le y \le l,\ z = -h/2, \tag{2.8}$$

$$\begin{cases} \dfrac{\partial H_z}{\partial y} - \dfrac{\partial H_y}{\partial z}\Big|_{I} = \dfrac{\partial H_z}{\partial y} - \dfrac{\partial H_y}{\partial z}\Big|_{II} \\ -\dfrac{\partial H_z}{\partial x} - \dfrac{\partial H_x}{\partial z}\Big|_{I} = \dfrac{\partial H_z}{\partial x} - \dfrac{\partial H_x}{\partial z}\Big|_{II} \end{cases} \text{ at } z = h/2, \tag{2.9}$$

$$H_y^{I} = H_y^{II} \text{ at } 0 \le x \le w,\ 0 \le y \le l,\ z = h/2. \tag{2.10}$$

In addition to the boundary condition, we use $\nabla \cdot H = 0$. Using the relations presented above we obtained four coupled matrix equations for four unknown vectors (G,F,A, and B). Here are the solution to the Fourier amplitudes [1]

$$A = \frac{1}{2\left(W_x \cot\frac{\mu h}{2} - \frac{i\mu}{k\pi}\right)}, \tag{2.11}$$

$$B = -\frac{1}{2\left(W_x \tan\frac{\mu h}{2} + \frac{i\mu}{k\pi}\right)}, \tag{2.12}$$

$$F_{mn}^{y} = \frac{\chi_{mn}^2 + \alpha_{mn}^2}{\chi_{mn} k} \times K_{mn} \frac{\frac{i\mu}{k\pi}}{\left(W_x^2 + \left(\frac{\mu}{k\pi}\right)^2\right)\sin\mu h + 2\frac{i\mu}{k\pi} W_x \cos\mu h}, \tag{2.13}$$

$$G_{mn}^{y} = 1 - \frac{\chi_{mn}^2 + \alpha_{mn}^2}{\chi_{mn} k} \times K_{mn} \frac{W_x + \frac{i\mu}{k\pi}\cot\mu h}{\left(W_x^2 + \left(\frac{\mu}{k\pi}\right)^2\right)\sin\mu h + 2\frac{i\mu}{k\pi} W_x \cot\mu h}. \tag{2.14}$$

We can now work our way back to find the magnetic and electric fields in any of the three regions. The near electric field in the transmission region is then given by:

$$E_x^{III} = \sqrt{\frac{\epsilon_0}{\mu_0}} \sum_{mn} \left(K_{mn} \frac{W_x + \frac{i\mu}{k\pi} \cot \mu h}{\left(W_x^2 + \left(\frac{\mu}{k\pi} \right)^2 \right) + 2W_x \frac{i\mu}{k\pi} \cot} \right) e^{i\chi_{mn}\left(z - \frac{h}{2}\right)} \times e^{i(\phi_{mn} - \omega t)}, \tag{2.15}$$

$$E_Y^{III} = 0, \tag{2.16}$$

$$E_z^{III} = \sqrt{\frac{\epsilon_0}{\mu_0}} \sum_{mn} \left(\frac{\alpha_{mn}}{\chi_{mn}} K_{mn} \frac{\frac{i\mu}{k\pi}}{\left(W_x^2 + \left(\frac{\mu}{k\pi} \right)^2 \right) \sin \mu h + 2W_x \frac{i\mu}{k\pi} \cot \mu h} \right) e^{i\chi_{mn}\left(z - \frac{h}{2}\right)} \times e^{i(\phi_{mn} - \omega t)}. \tag{2.17}$$

Other resonance phenomena such as surface plasmon polariton excitation [5], Fabry-Perot resonance [6] have been shown to accumulate the energy of incident light trough subwavelength structure.

2.3 Field Enhancement

In addition to creating a resonance behavior, rectangular hole arrays in thin metal films enhance the near electric field. When an EM wave hits a metal plane at normal incidence it will induce current on the surface of the plane. The current reflects lights back and none of the charges are accumulated in the metal. It becomes interesting when the plane is cut in two pieces, charges will then accumulate at the edges. When both edges are far apart the charge density is low, but when the two planes are brought together the charges start experiencing the pull from the charges on the other edge. This is visually represented in Figure 2.2. As more charges accumulate, the interaction becomes stronger and they move closer to the edges, enhancing the near electric field. It becomes obvious then that the strength of the near-field is inversely proportional to the width of the antenna.

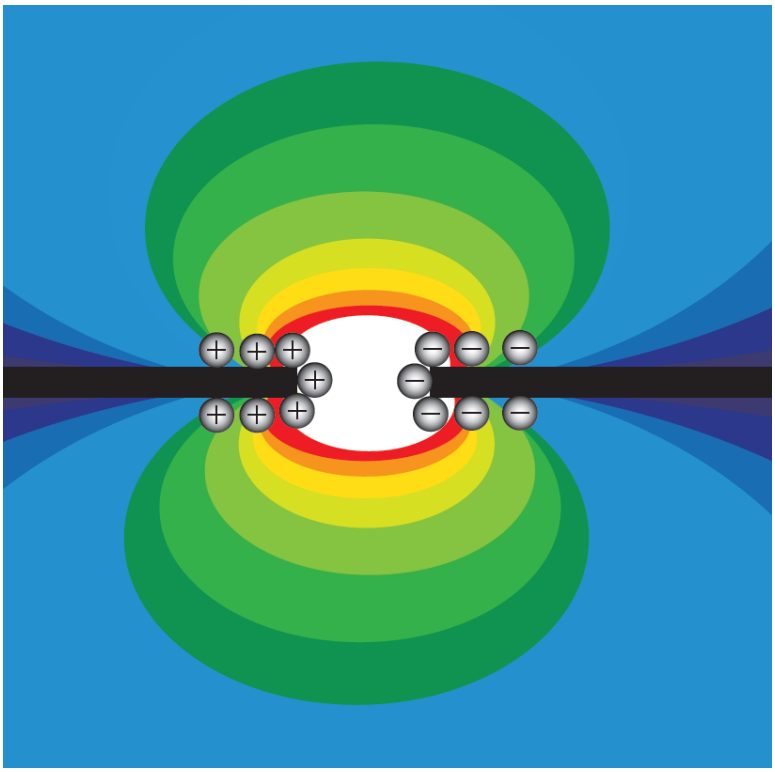

Figure 2.2: **Enhanced electric field** representation due to charge accumulation at the aperture. The colour contour is a visual aid and is not proportional to the field enhancement.

The field enhancement depends primarily on the coverage of the nanoantennas [7, 1]. The area-normalized amplitude is inversely proportional to the width of the rectangular hole. As the gap of the hole becomes smaller the near field is greatly enhanced [8]. We use the results that were found in section 2.2 to find expressions for the near-field and the far-field that are the electric field in region II and III, respectively. The near-field at the center of the slot is given by,

$$E_{\text{near}}(x = w/2, y = l/2, z = h/2) = \frac{\frac{i\mu}{k\pi}}{\left(W_x^2 + \left(\frac{\mu}{k\pi}\right)^2\right) + 2W_x \frac{i\mu}{k\pi} \cot \mu h} e^{-i\omega t}. \tag{2.18}$$

Then the far-field is described by,

$$E_{\text{far}} = \frac{\frac{i\mu}{k\pi}}{\left(W_x^2 + \left(\frac{\mu}{k\pi}\right)^2\right) + 2W_x \frac{i\mu}{k\pi} \cot \mu h} \frac{2}{\pi} \frac{lw}{d_x d_y} e^{i(k_0 z - \omega t)}. \tag{2.19}$$

This equation is crucial as we observe that the far-field is proportional to the coverage which is defined as the fraction of the area of the rectangular hole divided by the total film area $\beta = lw/d_x d_y$. Finally we can see that by dividing the real part of equation 2.18 by the real part of equation 2.19 we can obtain a simple expression that will relate the near-field to the far-field.

$$\frac{|E_{\text{near}}|}{|E_{\text{far}}|} = \frac{\pi}{2}\frac{d_x d_y}{lw} \tag{2.20}$$

$$E_{\text{near}} = \frac{\pi}{2}\frac{1}{\beta}|E_{\text{far}}| \tag{2.21}$$

The field enhancemnet factor is defined by the ratio of the near field to the incident field $\alpha = E_{\text{near}}/E_{\text{inc}}$. Substituting equation 2.21 yields:

$$\alpha = \frac{\pi}{2}\frac{1}{\beta}\frac{|E_{\text{far}}|}{|E_{\text{inc}}|} \tag{2.22}$$

This expression allow us to calculate the field enhancement from our measurements of the incident field and the transmitted far-field and the characteristic dimensions of the sample. Even though the path to obtain this electric field is rather convoluted, the mechanism can be fairly easily modeled.

Chapter 3

High-Field Terahertz Spectroscopy

3.1 Experimental Setup

In order to study the THz nanoantennas we employ high-field THz time-domain spectroscopy, the shecmatic of the setup used is shown in Figure 3.1. The high intensity THz pulses are generated using a 1 kHz Ti-Sapphire amplifier. The optical pump pulses have an energy of 1 mJ with a duration of 120 fs at a wavelength of 800 nm. The original beam is consecutively split into three different beams. The first beam splitter reflects 5% of the original beam. This first reflected beam is used for THz detection where the THz waveform will be recorded by electro optic sampling using a 1 mm thick ZnTe crystal. The second beam splitter reflects 10% of the 95% remaining from the previous beam splitter. This second reflected beam is used for optical excitation of the sample. The main beam is used for THz generation and is then collimated using parabolic mirrors. THz radiations are generated by optical rectification inside a nonlinear crystal. The crystal used in our experiment is a lithium niobate (LiNbO3) prism. However, to obtain an efficient THz generation the group velocity of the ultrashort light pulse and the phase velocity of the THz radiation must be matched. A diffraction grating is used to tilt the pulse of the main beam before entering a lithium niobate crystal. Tilting the pulse front ensures that the velocity matching condition is met [4]. The spectrum of the THz is centered at 0.9 THz and has a bandwidth of 0.8 THz. The THz beam diameter was found to be 0.45 mm at the sample using knife-edge technique. This same method was used to find the diameter of the optical pump used for optical excitation. The optical pump

diameter was 3 mm. The half wave plate was used to vary the intensity of the incident THz field.

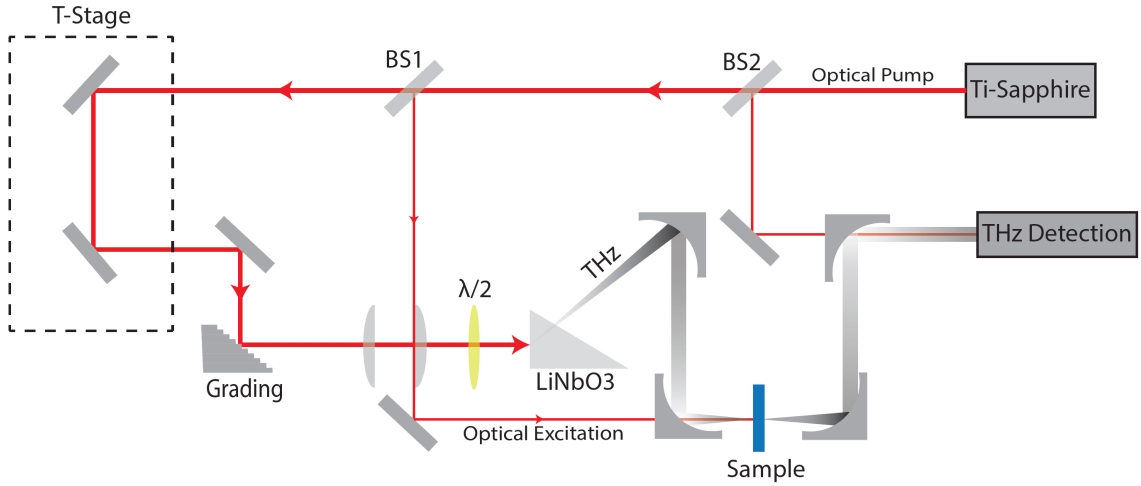

Figure 3.1: **Experimental set up** THz generation by tilted-pulse-front optical rectification in a LiNbO3 prism and THz time domain spectroscopy

Before generating THz pulses, the optical pump goes through a delay stage. The two mirrors are placed onto a translational stage (T-stage) that can be controlled to change the arrival time of the THz pulses. Then both the amplitude and the phase of the THz waveform can be mapped out as a function of time by the opticlal probe pulses. This method is called time domain spectroscopy and can provide more information than traditional Fourier-transform spectroscopy, which is not sensitive to the phase of the waveform.

3.2 Spectrum and Relative Transmission

3.2.1 Patterned Sample

Figure 3.2 shows the transmitted THz electric field as a function of time.

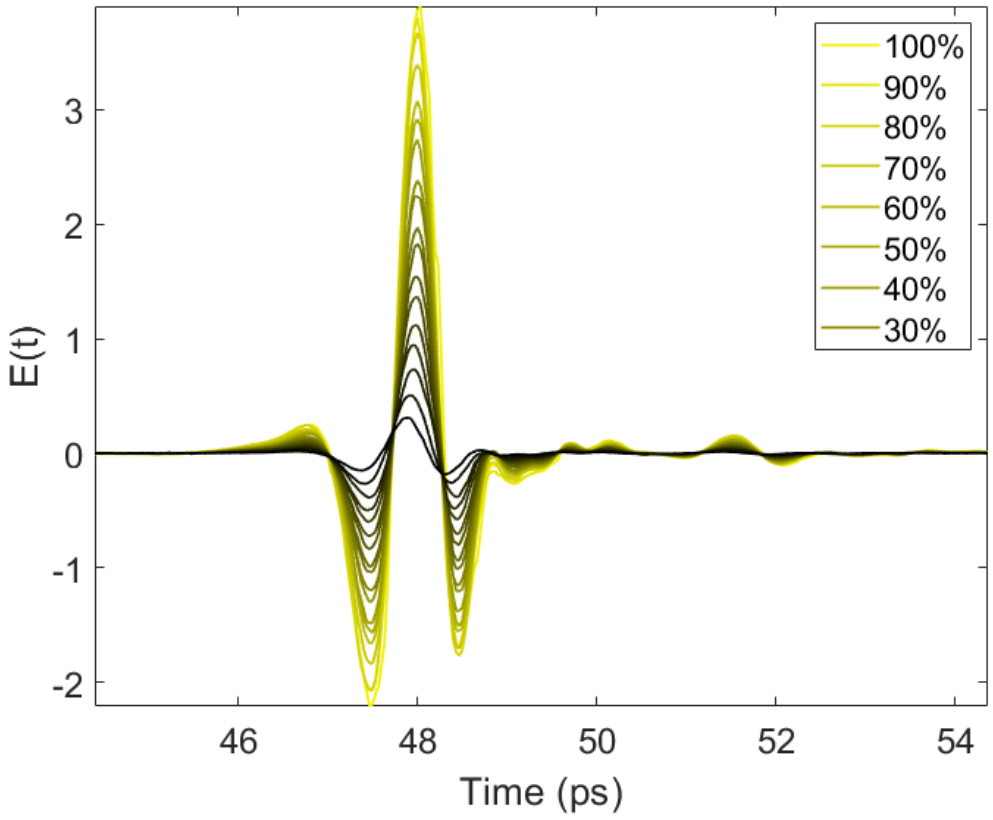

Figure 3.2: **Waveform** of the THz pulse after travelling through the sample.

We started the analysis of the experimental data by taking the Fourier transform of electric fields recorded. The transmission of the THz field was found by using $T = (|E_{far}|/|E_{air}|) \cdot \tau$, where τ is the pulse duration ratio of the transmitted pulse and the incident pulse. As the THz radiation travels through the sample it gets stretched and is longer than the original one. This ratio was calculated by taking the ratio of the two pulse width in the frequency domain and is $\tau = 2.5$. Figure 3.3 shows the normalized transmission to air of the nanoantenna GaAs sample in the frequency domain. We can observe that the antenna resonance occurs at about 0.85 THz. More significant is the increase in absorption as the THz fields become more intense.

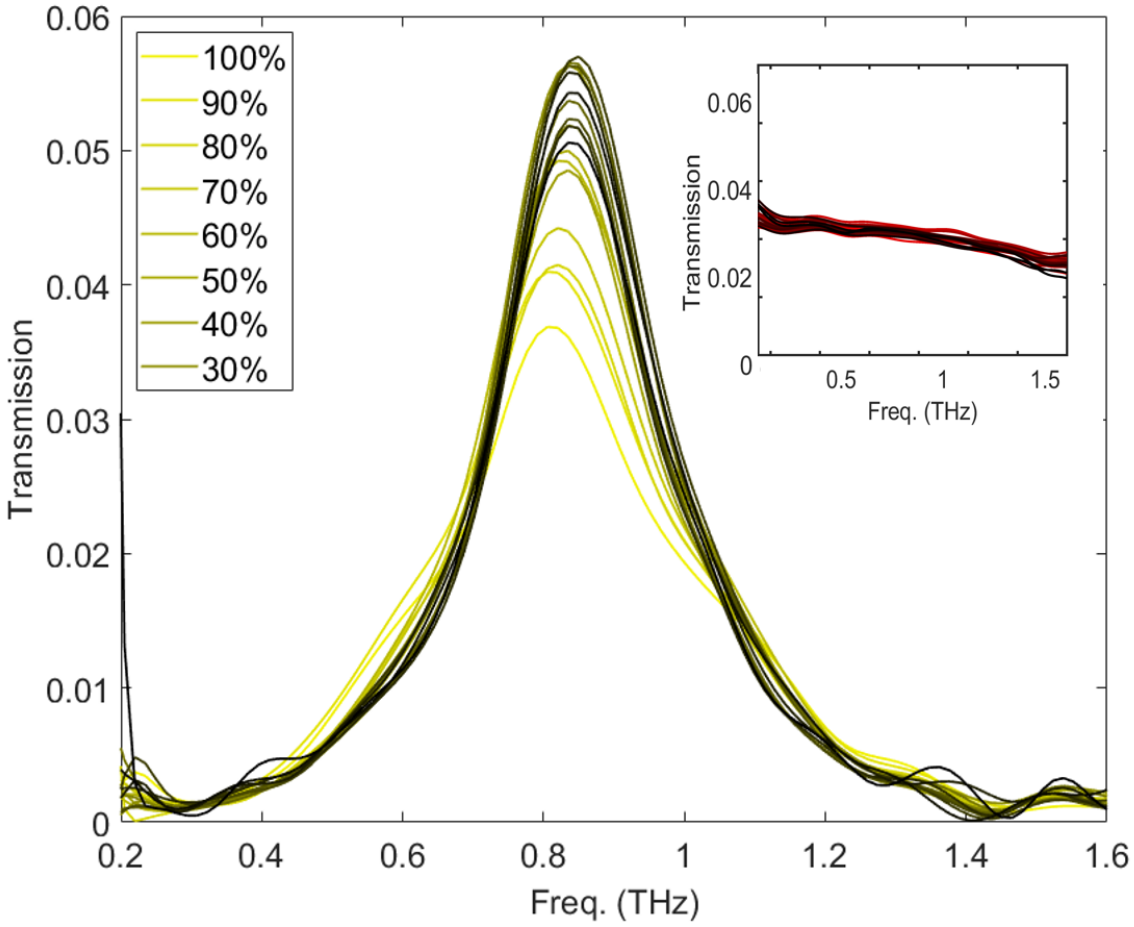

Figure 3.3: **Transmission Spectrum** of varying THz intensity on nanoantenna patterned GaAs. The inset shows the trasnmission spectrum for the bare GaAs.

3.3 Field Enhancement and Free Carrier Density

The experiment that was carried out yielded two main results. First, is the large field enhancement at the resonance frequency due to the nanoantennas. Second, the intense THz field generated by the field enhancement spawns free carriers inside GaAs. The free carrier generation being a result of the field enhancement occurring within the nanoantennas we will present the results in a similar order.

Figure 3.4 shows the field enhancement factor α as a function of the incident THz field intensity. The intensity of the field was varied using a polarizer. We observe that the enhancement remains fairly constant up to 55% of THz intensity. As the THz radiation

become more intense the enhancement decreases by almost 20%. We used Equation 2.22 to calculate the enhancement factor, the incident electric field data E_{far} was obtained by measuring the THz radiation with no sample in place while the far electric field was recorded with the sample. The coverage of this specific sample is $\beta = 1/350$. This drop in the field enhancement is in agreement with the decrease in transmission we observed in figure 3.3. This significant drop in the field enhancement suggest some kind of saturation process that occurs when th THz radiation becomes intense.

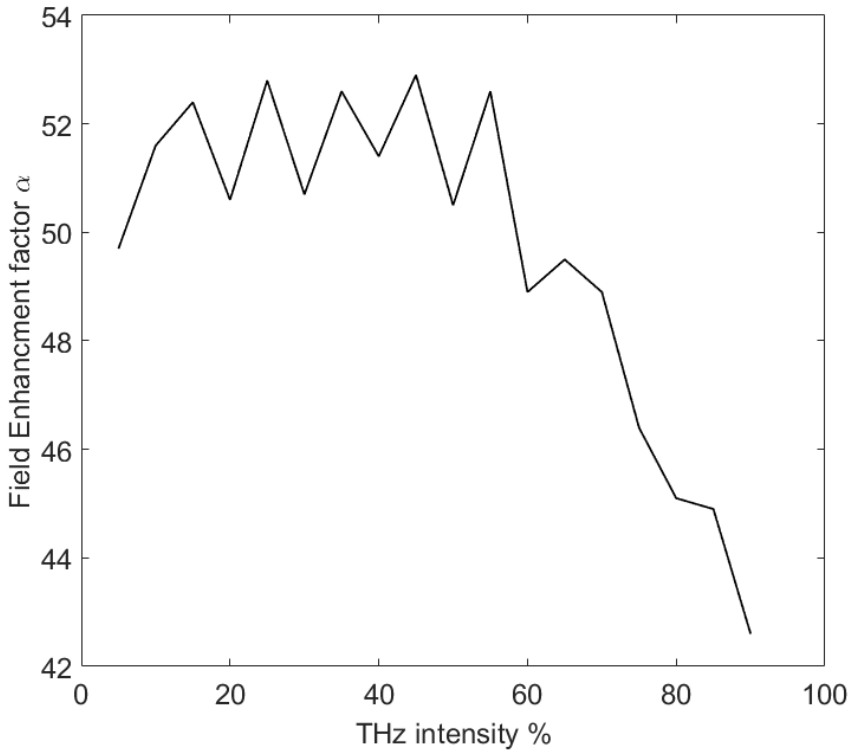

Figure 3.4: **Field Enhancement** starts decreasing as THz intensity increases.

From the results shown in figure 3.4 it then seemed of interest to study the free carriers dynamics inside the GaAs. Most of the THz absorption occurs predominantly in the nanometer-scale layer ($d_{\text{eff}} \approx w = 200nm$) [7]. This is due to the exponential decay of the near field amplitude in the direction normal to the gold/GaAs boundary. One method then to analyze the nonlinear THz absorption is to consider the nanometer-scale layer as a thin conduction film and to apply Fresnel thin film formula to acquire the THz induced conductivity. This approximation is reasonable as the GaAs wafer is thicker than the nanometer scale layer by several orders of magnitude (1/2500). After simplification the conductivity can be expressed in terms of the normalized nonlinear transmission ($T_{\text{rel}}(E_{\text{THz}}) = T(E_{\text{THz}})/T_0$) [7].

$$\sigma(E_{\text{THz}}) = \frac{n_G + 1}{Z_0 d_{\text{eff}}} \left[\frac{1}{\sqrt{T_{\text{rel}}(E_{\text{THz}})}} - 1 \right]. \tag{3.1}$$

where $Z_0 = 376.7\Omega$ is the vacuum impedance, and $n_G = 3.6$ is the index of refraction inside GaAs in the THz regime. The free electron density can then be found from the relation between their mobility and the conductivity: $\sigma(E_{\text{THz}}) = N_e(E_{\text{THz}})e\mu_e$ where $N_e(E_{\text{THz}})$ is the electron density, e is the electron charge and $\mu_e \cong 6 \times 10^3 \text{cm}^2/Vs$ is the electron mobility. Consequently, the electron density becomes:

$$N_e(E_{\text{THz}}) = \frac{\sigma(E_{\text{THz}})}{e\mu_e}. \tag{3.2}$$

The calculations of the electron density as a function of the incident THz field intensity are shown in Figure 3.5. In an opposite manner to the field enhancement the electron density sharply increases around 55% of intensity. This sudden increase indicates that intense THz radiation generates high density free carriers. This is in good agreement with our results presented in figure 3.4, as the THz field becomes more intense it generates more free carriers which eventually saturate the enhancement effect.

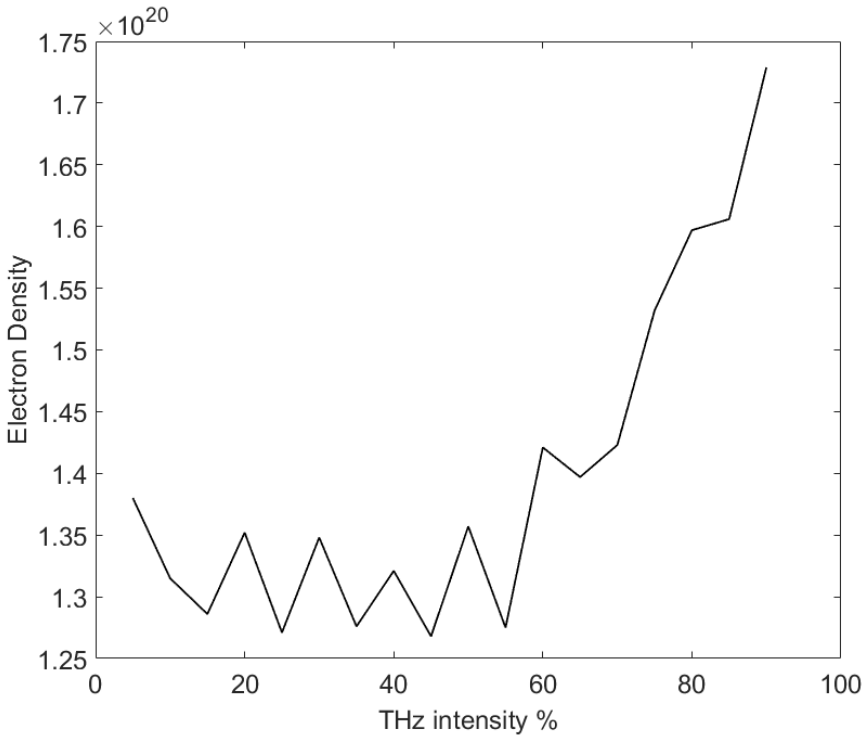

Figure 3.5: **Electron Density** of varying THz intensity on nanoantenna patterned GaAs

We have seen above that as the THz field becomes stronger the transmission decreases significantly. The electrons from the intense THz field have enough kinetic energy to knock the electron out of the valence band to the conduction band inside gallium arsenide. This phenomenon of impact ionization generates high density free carriers which consequently induce high THz absorption. Anterior studies have shown that in lower THz regime ($\sim$ 100 kV/cm) the principal mechanism that generate free carrier is an intraband process; however, in higher THz regime such as the one displayed in this paper the THz field exhibit nonlinear effects that generates free carriers via interband transition [7]. Another possible mechanism repsonisble for the generation of free carriers in GaAs is Zener tunneling which occurs when the incident electric field is strong enough.

Chapter 4

Conclusion

The recent development in the generation of intense THz fields has made new studies of electron dynamics in semiconductors more accessible. More specifically, gallium arsenide is a semiconductor that has high saturated electron velocity which suggest its application in ultra-fast electronics. Another recent method was designed to enhance even further the intensity of the near field THz radiation by using an array of small rectangular holes. Those nanoantennas enables researchers to study semiconductors in the high field regime.

In this project we used high-field THz time-domain spectroscopy to investigate the effects of THz nanoantennas on a GaAs wafer. We observed that the absorption of the THz pulses increases as their intensity increased. Similarly, we notices that the near-field enhancement factor due to the nanoantennas decreased by 20% at about 60% of the incident intensity. We studied the electron density on the GaAs wafer as a function of THz intensity and observed that as the THz became more intense the carrier density increased up to 10^{20}cm^{-3}. We concluded that the nanoanttena array caused a huge near field enhancement which generated high density free carriers by interband excitation which induced nonlinear THz absorption in the GaAs.

According to previous work impact ionization is the most probable mechanism responsible for the generation of high density free carriers. Other studies have suggested the Zener tunneling is also a good candidate. The origin of the of the THz free electrons is still unclear and is a great motive to investigate further the properties of semiconductor. Additionally, using nanoantenna array to enhance the near field is a cheap and adaptable

technique that couple very well with THz spectroscopy.

Bibliography

[1] D. Park, S. Choi, Y. H. Ahn, Q.-H. Park, and D. Kim, "Theoretical study of terahertz near-field enhancement assisted by shape resonance in rectangular hole arrays in metal films," Journal of the Korean Physical Society, vol. 54, pp. 64–70, 01 2009.

[2] F. J. García-Vidal, E. Moreno, J. A. Porto, and L. Martín-Moreno, "Transmission of light through a single rectangular hole," Phys. Rev. Lett., vol. 95, p. 103901, Aug 2005.

[3] Y.-S. Lee, Tabletop High-Power Terahertz Pulse Generation Techniques, pp. 29–46. 06 2014.

[4] A. G. Stepanov, J. Hebling, and J. Kuhl, "Efficient generation of subpicosecond terahertz radiation by phase-matched optical rectification using ultrashort laser pulses with tilted pulse fronts," Applied Physics Letters, vol. 83, no. 15, pp. 3000–3002, 2003.

[5] W. L. Barnes, W. A. Murray, J. Dintinger, E. Devaux, and T. W. Ebbesen, "Surface plasmon polaritons and their role in the enhanced transmission of light through periodic arrays of subwavelength holes in a metal film," Phys. Rev. Lett., vol. 92, p. 107401, Mar 2004.

[6] Y.-H. Ye, Y.-W. Jiang, M.-W. Tsai, Y.-T. Chang, C.-Y. Chen, D.-C. Tzuang, Y.-T. Wu, and S.-C. Lee, "Localized surface plasmon polaritons in agsio2ag plasmonic thermal emitter," Applied Physics Letters, vol. 93, no. 3, p. 033113, 2008.

[7] Y.-G. Jeong, M. J. Paul, S.-H. Kim, K.-J. Yee, D.-S. Kim, and Y.-S. Lee, "Large enhancement of nonlinear terahertz absorption in intrinsic gaas by plasmonic nano antennas," Applied Physics Letters, vol. 103, no. 17, p. 171109, 2013.

[8] D. J. Park, S. B. Choi, Y. H. Ahn, F. Rotermund, I. B. Sohn, C. Kang, M. S. Jeong, and D. S. Kim, "Terahertz near-field enhancement in narrow rectangular apertures on metal film," Opt. Express, vol. 17, pp. 12493–12501, Jul 2009.